Gastroenterology 2023;165:1180–1196

INFLAMMATORY BOWEL DISEASE

Stricturing Crohn's Disease Single-Cell RNA Sequencing Reveals Fibroblast Heterogeneity and Intercellular Interactions

Pranab K. Mukherjee,[1,9] Quang Tam Nguyen,[1,9] Jiannan Li,[1] Shuai Zhao,[1] Stephen M. Christensen,[2] Gail A. West,[1] Jyotsna Chandra,[1,9] Ilyssa O. Gordon,[3,9] Sinan Lin,[1,4] Jie Wang,[1,5] Ren Mao,[1,4] Douglas Czarnecki,[1] Carla Rayan,[1] Idan Goren,[1] Suhanti Banerjee,[1] Prerna Kotak,[6] Thomas Plesec,[3,9] Samir Lal,[2] Thomas Fabre,[2] Shoh Asano,[2] Kathryn Bound,[2] Kevin Hart,[2] Chanyoung Park,[2,10] Robert Martinez,[2] Ken Dower,[2] Thomas A. Wynn,[2] Shaomin Hu,[3,9] Nayden Naydenov,[1] Martin Decaris,[6] Scott Turner,[6] Stefan D. Holubar,[7,9] Scott R. Steele,[7] Claudio Fiocchi,[1,8] Andrei I. Ivanov,[1,9] Kellie M. Kravarik,[2] and Florian Rieder[1,8,9]

[1]Department of Inflammation and Immunity, Lerner Research Institute, Cleveland Clinic, Cleveland, Ohio; [2]Worldwide Research, Development and Medicine, Pfizer Inc, Cambridge, Massachusetts; [3]Department of Pathology, Robert J. Tomsich Pathology and Laboratory Medicine Institute, Cleveland Clinic Foundation, Cleveland, Ohio; [4]Department of Gastroenterology and Hepatology, The First Affiliated Hospital of Sun Yat-sen University, Guangzhou, China; [5]Henan Key Laboratory of Immunology and Targeted Drug, Xinxiang Medical University, Xinxiang, Henan Province, China; [6]Pliant Therapeutics, South San Francisco, California; [7]Department of Colorectal Surgery, Digestive Disease and Surgery Institute, Cleveland Clinic, Cleveland, Ohio; [8]Department of Gastroenterology, Hepatology and Nutrition, Digestive Disease Institute, Cleveland Clinic, Cleveland, Ohio; [9]Center for Global Translational Inflammatory Bowel Disease Research, Cleveland Clinic, Cleveland, Ohio; and [10]Department of Biology, Massachusetts Institute of Technology, Cambridge, Massachusetts

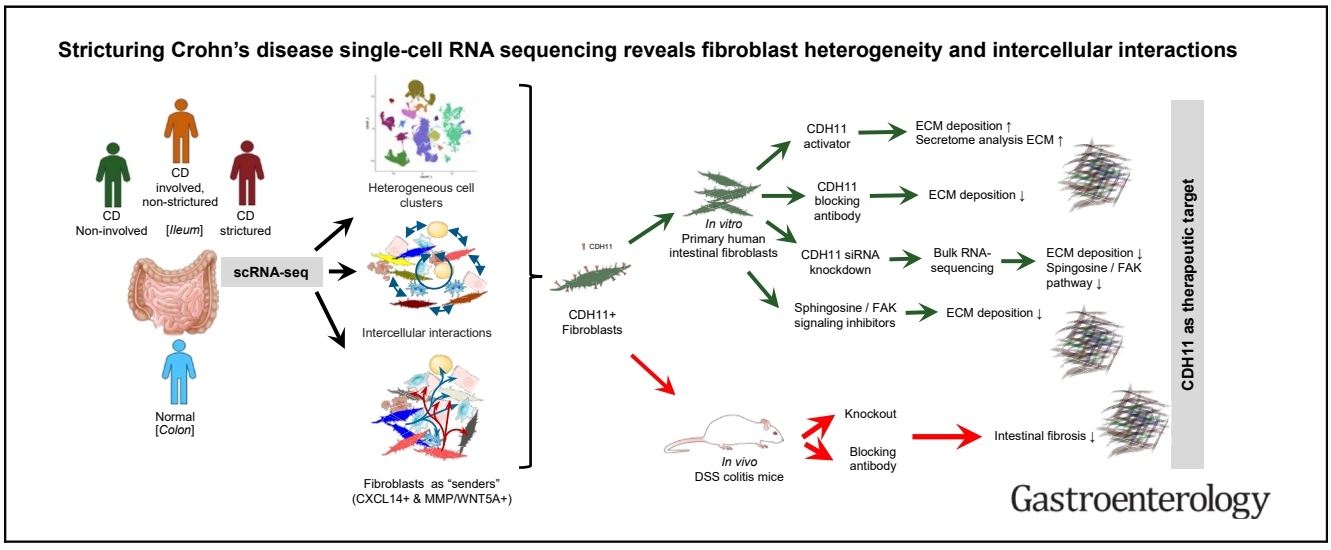

BACKGROUND & AIMS: Fibroblasts play a key role in stricture formation in Crohn's disease (CD) but understanding its pathogenesis requires a systems-level investigation to uncover new treatment targets. We studied full-thickness CD tissues to characterize fibroblast heterogeneity and function by generating the first single-cell RNA sequencing (scRNAseq) atlas of strictured bowel and providing proof of principle for therapeutic target validation. **METHODS:** We performed scRNAseq of 13 fresh full-thickness CD resections containing noninvolved, inflamed nonstrictured, and strictured segments as well as 7 normal non-CD bowel segments. Each segment was separated into mucosa/submucosa or muscularis propria and analyzed separately for a total of 99 tissue samples and 409,001 cells. We validated cadherin-11 (CDH11) as a potential therapeutic target by using whole tissues, isolated intestinal cells, NanoString nCounter, next-generation sequencing, proteomics, and animal models. **RESULTS:** Our integrated dataset revealed fibroblast heterogeneity in strictured CD with the majority of stricture-selective changes detected in the mucosa/submucosa, but not the muscle layer. Cell-cell interaction modeling revealed CXCL14+ as well as MMP/WNT5A+ fibroblasts displaying a central signaling role in CD strictures. CDH11, a fibroblast cell-cell adhesion molecule, was broadly expressed and upregulated, and its profibrotic function was validated using NanoString nCounter, RNA sequencing, tissue target expression, in vitro gain- and loss-of-function experiments, proteomics, and

knock-out and antibody-mediated CDH11 blockade in experimental colitis. **CONCLUSIONS:** A full-thickness bowel scRNAseq atlas revealed previously unrecognized fibroblast heterogeneity and interactions in CD strictures and CDH11 was validated as a potential therapeutic target. These results provide a new resource for a better understanding of CD stricture formation and open potential therapeutic developments. This work has been posted as a preprint on Biorxiv under doi: 10.1101/2023.04.03.534781.

Keywords: Stricture; Crohn's; Therapy; Single Cell.

Inflammatory bowel diseases (IBD) are a group of chronic inflammatory disorders that include Crohn's disease (CD) and ulcerative colitis (UC).[1] A major complication of CD is intestinal fibrosis leading to stricture formation, the main cause for surgical interventions.[2] Conventional anti-inflammatory therapies can only modestly reduce the occurrence of stricturing disease[3,4] and no anti-fibrotic or selective anti-stricture therapy is available, making this a significant clinical problem.

Mesenchymal cells, the major effector cell in intestinal fibrosis,[5] represent a distinctive cell population where fibroblasts are the predominant cell type. In the strictured bowel of patients with CD, fibroblasts become activated, increase in number, and produce excessive extracellular matrix (ECM). In addition, under inflammatory conditions like CD, mesenchymal cells interact intimately with each other as well as with nearby immune and nonimmune cells,[5] leading to complex fibrogenic circuits. Until now the understanding of such circuits has been hindered by the traditional classification of mesenchymal cells into fibroblasts, myofibroblasts, and smooth muscle cells (SMCs),[6] which lacks specificity.

A better understanding of the multifaceted cellular networks underlying fibrogenesis and stricture formation in CD requires high-resolution molecular profiling, such as single-cell RNA sequencing (scRNAseq).[5] This approach has revealed distinct changes in the epithelial, immune, and stromal cell compartments in both UC[7,8] and CD.[9] However, as innovative as it is, the obtained information was derived from superficial endoscopic mucosal biopsies which, given the transmural nature of CD, fail to comprehensively capture the complexity of intestinal fibrogenesis, which can only be fully appreciated by studying it in all intestinal tissue layers. Therefore, to comprehensively examine the transmural changes in CD and differentiate possible cellular subtypes in strictured (CDs), nonstrictured (CDi), and noninvolved (CDni) tissues, we leveraged scRNAseq and transcriptomic signatures in a well-phenotyped cohort of CD and control surgically resected intestinal tissues.

Our approach identified previously unrecognized mesenchymal cell populations, distinct cell niches, and related cell interactions in strictured CD bowel. We identified differentially expressed genes and pathways, and comprehensive in vitro and in vivo studies demonstrated that cadherin-11 (CDH11) is a fibroblast-selective surface molecule with prominent profibrotic properties.

WHAT YOU NEED TO KNOW

BACKGROUND AND CONTEXT

Stricturing Crohn's disease (CDs) is a significant clinical problem and fibroblasts play a key role in its pathogenesis. We created a single-cell RNA sequencing (scRNAseq) atlas of strictured bowel and controls.

NEW FINDINGS

Sequencing 409,001 cells, we revealed previously unrecognized fibroblast heterogeneity, interactions and CXCL14+ & MMP/WNT5A+ fibroblasts displaying a central signaling role in CD strictures. Cadherin-11 (CDH11) was validated as a potential therapeutic target.

LIMITATIONS

Our surgical cohort represents late and already established disease. We are not able to elucidate a link of medications at time of surgery with the findings.

CLINICAL RESEARCH RELEVANCE

An increasing understanding of CDs, a complication for which no selective therapies exist, can lead to development of novel antifibrotic treatments. Blockade of CDH11 may be tested in clinical trials for CDs.

BASIC RESEARCH RELEVANCE

These results provide a new resource for a better understanding of CD stricture formation. The scientific community and industry can use this dataset to generate or validate hypotheses and develop novel therapeutic drug targets.

Methods

Tissue Procurement

Briefly, full-thickness freshly resected intestinal specimens from subjects with CD and controls, comprising apparently healthy tissue (constipation, healthy margin of resections from patients with intestinal cancer; termed "NL" for normal) were procured as previously described.[10,11] This protocol was approved by the Cleveland Clinic Institutional Review Board (number 17-1167). Before resection in patients with CD, the presence of a stricture was ascertained using cross-sectional imaging (computed tomography or magnetic resonance imaging) and/or inability to pass an adult or pediatric

Abbreviations used in this paper: **α-SMA, alpha-smooth muscle actin; AKT, a serine/threonine protein kinase; CCL, C-C motif chemokine ligand; CD, Crohn's disease; CDi, nonstrictured but inflamed Crohn's disease; CDni nonstrictured, noninflamed Crohn's disease; CDns, ileal Crohn's disease nonstricturing; CDs, strictured CD; CDH11, Cadherin-11; DES, desmin; CXCL, chemokine (C-X-C motif) ligand; DSS, dextran sodium-sulfate; ECM, extracellular matrix; FAK, focal adhesion kinase; FFPE, formalin-fixed paraffin embedded; FN, fibronectin; GAPDH, glyceraldehyde-3-phosphate dehydrogenase; HIMFs, human intestinal myofibroblasts; IBD, inflammatory bowel disease; Ig, immunoglobulin; IL, interleukin; KD, knockdown; KO, knockout; LP, lamina propria; mTOR, mammalian target of rapamycin; MP, muscularis propria; NL, non-IBD patients; RNAseq, RNA sequencing; scRNAseq, single-cell RNA sequencing; SES-CD, Simple Endoscopic Score for Crohn's Disease; SMC, smooth muscle cell; TGF, transforming growth factor; TNF, tumor necrosis factor; UC, ulcerative colitis; WT, wild type.**

Most current article

0016-5085/$36.00
https://doi.org/10.1053/j.gastro.2023.07.014

ileocolonoscope. Postresection, CD specimens were classified based on gross anatomy into segments of CDs, CDi (purely inflammatory disease without the presence of stricture), and CDni (noninflammatory disease without the presence of stricture). For generation of the scRNAseq atlas (following manufacturer's instructions and as described in Supplementary Methods and chemistries shown in Supplementary Table 1), the 3 CD segments were from the same patient's resection. Each segment was scored and characterized using a macroscopic score modified from the simple endoscopic score–CD[10] and a histopathologic score for inflammation[11] or fibrosis[12] (Supplementary Tables 2 and 3). This procurement system was validated using macroscopic and histopathologic evaluation performed by a trained IBD pathologist (I.O.G.). The time from resection in the operating room to starting tissue processing in the laboratory was <30 minutes.

ECM Deposition Assay for Human Intestinal Myofibroblasts

Deposition of ECM by intestinal myofibroblasts was assayed using modification of a method described previously.[13] Briefly, recombinant human CDH11-Fc chimera (CDH11Fc, R&D Systems; catalog number 1970-CA) or H1M1 antibody (prepared from hybridoma PTA-9699 [ATCC] *at high purity [>99%] and low endotoxin levels [<0.23 EU/mg]*) were used as activator and as a functional blocker of CDH11 in human intestinal myofibroblasts (HIMF), respectively. A 96-well dark-walled imaging plate (Greiner, BioOne, catalog number 655090) was coated with CDH11Fc, H1M1, or human immunoglobulin (Ig)G1 or IgG2b isotype control, respectively, in phosphate-buffered saline for 2 hours at 37°C. HIMFs were plated (3200 cells/well) in Dulbecco's modified Eagle medium supplemented with 10% fetal bovine serum and antibiotics, and incubated overnight. Cells were then incubated with serum-free culture medium to produce ECM for 5 days and subsequently removed using 0.25 mol/L ammonium hydroxide in 50 mmol/L Tris pH 7.4. Deposited ECM was fixed by exposure to 100% methanol at −20°C and stained with Alexa Fluor488-conjugated anti-fibronectin (EBioscience, clone FN-3, 1:500 dilution) or Alexa Fluor594-conjugated (Invitrogen, 1:1000 dilution) anti-ColI/III antibodies (EMD, Millipore Corp., 1:100 dilution). Fluorescence intensities were obtained using a Cytation5 scanner (Agilent Biotek). The following compound inhibitors were used in the ECM deposition assay in conjunction with the HIMF: GSK690693 (pan-Akt inhibitor, Sigma-Aldrich, catalog number 937174-76-0), mTOR Inhibitor XI, Torin1 (Sigma-Aldrich, catalog number 1222998-36-8), LY-294,002 hydrochloride (Pi3K inhibitor, Sigma-Aldrich, catalog number 934389-88-5), Y15 (focal adhesion kinase [FAK] inhibitor, 1,2,4,5-benzenetetramine tetrahydrochloride, Sigma-Aldrich, catalog number 406-66-5), and SEW 2871.

Full information on tissue dissociation and isolation of single cells, library generation, scRNAseq analysis, cyclic immunofluorescence, quantitative reverse transcriptase polymerase chain reaction, immunostaining and quantification, immunofluorescence labeling and confocal microscopy, RNA extraction from formalin-fixed paraffin-embedded (FFPE) tissue, gene expression analysis using NanoString nCounter platform, isolation of primary human intestinal cells, cell cultures, immunoblotting, proteomics, RNA interference, next-generation RNA sequencing, antibodies, animals, dextran sodium-sulfate (DSS)–induced colitis, chronic DSS model with CDH11 blockade in BALB/c wild type (WT) mice, experimental fibrosis endpoints, and statistical analysis can be found in the Supplementary Materials.

The transcriptomic datasets will be shared on request. Please contact the corresponding author for any inquiries. The Cleveland Clinic agrees to use the National Institutes of Health's Federal Demonstration Partnership (FDP) Data Transfer and Use Agreement (DTUA) template to share the data, which can be found at https://thefdp.org/default/committees/research-compliance/data-stewardship/.

Results

A Single-Cell Atlas of Full-Thickness CD Reveals Shifts in Cell Type Composition From Noninvolved to Inflamed to Stricturing Phenotype

We generated a scRNAseq transcriptional atlas from 13 ileal CD full-thickness and 7 NL colonic tissues. CD resections were separated into CDni, CDi, and CDs segments when available, as described in the Methods section. We mechanically dissected the muscularis propria (MP) from the mucosa/submucosa, which was subsequently processed into an epithelial-enriched fraction (LP1) and a lamina propria-enriched fraction (LP2). We were not able to obtain all fractions and segments from all patients. If sufficient libraries were not obtained from particular samples, they are also missing from the final atlas. Neither of these pertained to a particular region or fraction. This resulted in a total of 99 analyzed fractions and 409,001 high-quality single-cell transcriptomes (Figure 1*A*); 97,954 cells were sequenced from CDni, 101,164 from CDi, 94,049 from CDs, and 115,834 from NL, with a median recovery of 471 genes/cell and 751 Unique Molecular Identifier/cell (Supplementary Figure 1*A*). The total number of obtained cells per fraction or segment did not correlate with the macroscopic inflammation score. In addition, the numbers for each individual obtained cell type per fraction and segment also did not correlate with the macroscopic inflammation score, with the exception of Goblet cells in CDs (Supplementary Table 6*A*). Samples from NL segments had slightly more cells sequenced per sample in the LP1 and LP2 regions compared with CD, but the number of cells per fraction were fairly similar across the atlas (Supplementary Table 6*B*). Overall preparation quality was high to excellent (viability >80%, mitochondrial reads <10% in more than 80% of cells; Supplementary Figure 1*B*).

Next, we broadly annotated the full dataset using canonical cell type markers and subclustered into epithelial, stromal, myeloid, B cell, and T/NK cell compartments (Figure 1*B*–*D*). The sequenced cell numbers per compartment and cell type can be found in Supplementary Table 6*C*. The subclustering resulted in 93 different cell types representative of the cell populations in each segment (Figure 1*C* and *D*). To investigate progression toward strictures, we examined differences in cell type composition by tissue type and layer (Figures 1*E* and *F*, Supplementary Figure 1*C*–*F*). Cell type composition of LP1 or LP2 vs MP was markedly different, but not between LP1 and LP2, which were thereafter combined as "LP1/2" (Supplementary Figure 1*C* and *D*). A detailed description of the changes in cell type and pseudobulk analysis between LP1, LP2, and MP can be

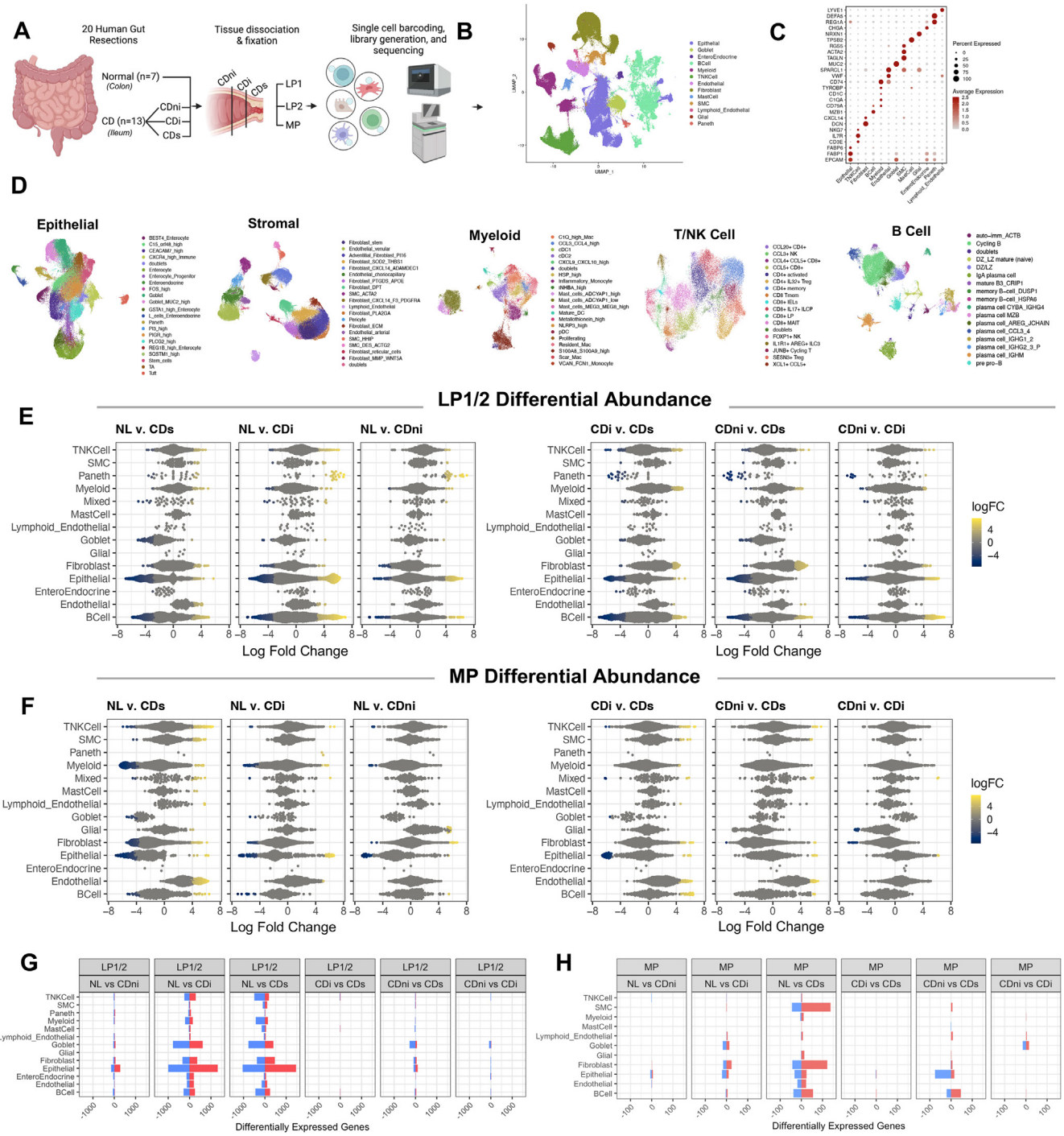

Figure 1. Generation of a full-thickness scRNAseq atlas. (*A*) Schematic summary of atlas generation from contributing donors. (*B*) Uniform manifold approximation and projection (UMAP) plot of all cells from the atlas colored by cell type. (*C*) Dot plot of canonical markers used to define and annotate general cell types. Average gene expression is shown by color intensity. Percent of cells expressing each gene is shown by size. (*D*) Compartmental UMAP plots for each subclustering analysis colored by cell types/states. (*E* and *F*) Differential abundance beeswarm plots from LP1/2 (*E*) or MP layer (*F*) layers by cell type. Each dot is a neighborhood of cells calculated using miloR. Neighborhoods that reach significance (spatial false discovery rate <0.1) are colored by log fold-change. (*G* and *H*) Bar plot representing the total number of up-regulated (*red*) or down-regulated (*blue*) genes by cell type in the LP1/2 (*G*) and MP (*H*) layers.

found in Supplementary Results and Supplementary Figure 1*C–F*. Consistent with progression from CDni to CDi, lymphocyte, myeloid, epithelial, and fibroblast cell composition was altered in CDi LP1/2 compared with CDni. Alteration in myeloid, lymphocyte, and epithelial cells was also evident in CDni compared with NL, suggesting the

influence of low-grade inflammation, an intrinsic disease-induced difference in CDni and/or difference in the colon or ileum origin of the tissue segment (Figure 1*E*). In the MP layer we found significant alteration of nearly all cell types in CDs compared with NL, with minor differences in CDi and CDni compared with NL. When comparing CDs with CDi in both LP1/2 and MP, we found significant differences of epithelial, lymphocyte, SMC, endothelial, fibroblast, and myeloid cell composition (Figure 1*E* and *F*).

In addition to cell type compositional changes related to disease progression, we examined general transcriptional changes using pseudobulk differential expression. Most differences between segments were observed in the LP1/2 layer, especially when comparing diseased with normal gut with the most marked in CDs compared with NL (Figure 1*G*). Epithelial cells in the LP1/2 layer exhibited the largest transcriptional changes with 2501, 2323, and 446 dysregulated genes in CDs, CDi, and CDni compared with NL, respectively. Fibroblasts also demonstrated an extensive transcriptional shift with disease progression in the LP1/2 layer with 842, 686, and 104 dysregulated genes in CDs, CDi, and CDni compared with NL, respectively. Surprisingly, only minor transcriptional changes in the MP layer were noted between segments, even when comparing CDs with all others (Figure 1*H*), suggesting that major compositional changes between segments were driven by the LP1/2 layers. Related signaling pathway perturbations were also noted (Supplementary Results and Supplementary Figure 2*A* and *B*)

Unique Cell Populations are Represented in the Stromal Compartment of CD Strictures

In the combined stromal compartment, we identified 19 distinct cell types primarily grouped into fibroblast, smooth muscle, and endothelial populations after subclustering analysis (Figure 2*A* and *B*). Among all mesenchymal cell types, only 4 were distinctly more abundant in the isolated LP1/2 layer (CXCL14/ADAMDEC1+, CXCL14/F3/PDGFRA+ and MMP/WNT5A+ fibroblasts and HHIP/NPNT+ SMCs), whereas the rest were more abundant in the isolated MP layer (Supplementary Figure 1*F*). Interestingly, 6 fibroblast populations (SOD2/THBS1+, PLA2GA+, PTGDS/APOE+, MMP/WNT5A+, fibroblast reticular cells, and ECM^{high}) were over-represented in CDs compared with both CDi and CDni in the LP1/2 layer, particularly in CDs vs CDni. These 6 fibroblast populations all express markers linked to fibrotic diseases via transforming growth factor (TGF)-b1 regulation, macrophage activation/differentiation, and ECM production. Among the fibroblast populations over-represented in CDs, only the MMP^{+}/WNT5A^{+} fibroblasts were more abundant in any segment vs NL, specifically in CDs compared with NL (Figure 2*C*). Conversely, the isolated MP layer showed minimal significant differences in cell population abundance when comparing CDs vs CDi. However, adventitial, stem-like, and SOD2/THBS1+ fibroblasts were under-represented and endothelial cells were over-represented in the isolated MP of CDs compared with NL (Figure 2*D*). Of note, differential abundance in cell types in CDs or differences in transcriptional activity per cell type in CDs held up when comparing CDs with NL or CDs or CDni. Together, these observations suggest the LP1/2 layer as a key pathogenic area of stricturing disease as evidenced by both the global and mesenchymal compositional and transcriptional alterations in disease.

Given these results, we next interrogated transcriptional changes within the stromal niche. Compatible with the global transcriptional view in Figure 1*G* and *H*, the LP1/2 layer contained the stronger perturbation of gene expression within each stromal cell type compared with the MP layer. Both CXCL14+ fibroblast populations as well as adventitial PI16+ fibroblasts had a large number of significantly differentially expressed genes when comparing CDs with CDni and NL, suggesting their contribution to stricture (Figure 2*E*). The stromal transcriptional changes in the MP layer were minimal, but most pronounced in CDs compared with NL segments. Cell types contributing to transcriptional changes were mainly stem-like fibroblasts and ACTA2+ SMCs (Figure 2*F*). The per cell type signaling pathways can be found in Supplementary Results and Supplementary Figure 3*A* and *B*. We further mapped previously published stromal populations associated with IBD onto our dataset and interrogated the frequency of the cell types per segment. These results can be found in Supplementary Results and Supplementary Figure 4*A* and *B*.

To understand global communications and interactions among cells we used CellChat[14] to quantitatively infer intercellular communication networks. CellChat predicts major signaling inputs (incoming receptor signals, received signals) and outputs (sent signals, outgoing signals) on a per cell type basis. Our initial analysis pointed to CDi and CDs as the most relevant areas underlying the progression from nonstrictured inflammation to stricture. In LP1/2 the major populations with strong incoming receptor signals in CDs compared with CDi are myeloid cell types (CLCL9/CXCL10^{high}, inflammatory monocytes, NLRP3^{high}, and Metallothionein^{high}), T/NK cells (CCL5/CD8+, CCL4/CCL5/CD8+, XCL1+, CCL5+), endothelial venular cells, MMP/WNT5A+ fibroblasts, and pericytes (Figure 3*A*). In the MP fraction, major populations that show strong incoming receptor signals are B cells (CCL3/4+ plasma cells, mature B3/CRIP1+, CYBA/IGHG4+ plasma cells), myeloid cells (cDC2, MEG3/MEG8^{high}, Metallothionein^{high}), and stromal cells (MMP/WNT5A+; Figure 3*C*). Strikingly, fibroblasts stand out as major signal senders in CDs compared with CDi in the LP1/2 layer, particularly CXCL14/ADAMDEC1+, MMP/WNT5A+, CXCL14/F3/PDGFRA+, and ECM^{high} cells (Figure 3*B*). A comparable finding was observed in the MP layer, with pericytes and SMC/HHIP+ stromal cells showing stronger outgoing signals in CDs compared with CDi. All other cell fractions had a negligible contribution as signal senders (Figure 3*D*). When evaluating the outgoing signal strength across segments in the stromal compartment the noted changes were found to be progressive with fibroblasts taking on an increasing signal sending role from NL, through CDni and CDi, to CDs (Figure 3*E*, Supplementary Figure 5). These findings indicate that fibroblasts are major "signal sending hubs" in CDs in the LP1/2 as well as MP layers.

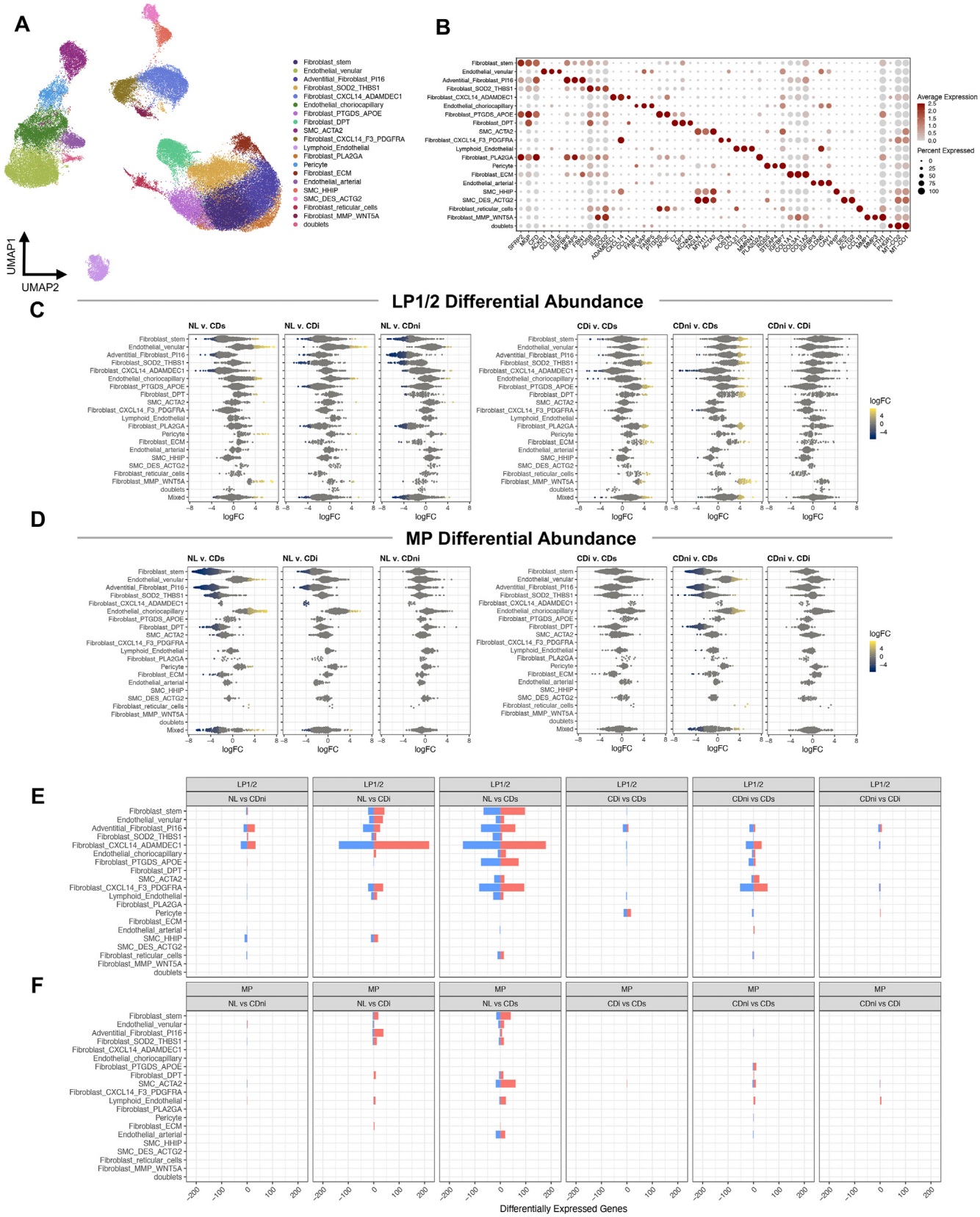

Figure 2. Stromal compartment analysis of the scRNAseq atlas. (*A*) UMAP plot of mesenchymal subclustering colored by cell type. (*B*) Dot plot of top markers used to define/annotate mesenchymal subsets. Average gene expression is shown by color intensity. Percent of cells expressing each gene is shown by size. (*C* and *D*) Differential abundance beeswarm plots from LP1/2 (*C*) and MP (*D*) layers by cell type. Each dot is a neighborhood of cells calculated using miloR. Neighborhoods that reach significance (spatial false discovery rate <0.1) are colored by log fold-change. (*E*) Bar plot representing the total number of up-regulated (*red*) or down-regulated (*blue*) genes by cell type in the LP1/2 layers (*F*) Bar plot representing the total number of up-regulated (*red*) or down-regulated (*blue*) genes by cell type in the MP layer.

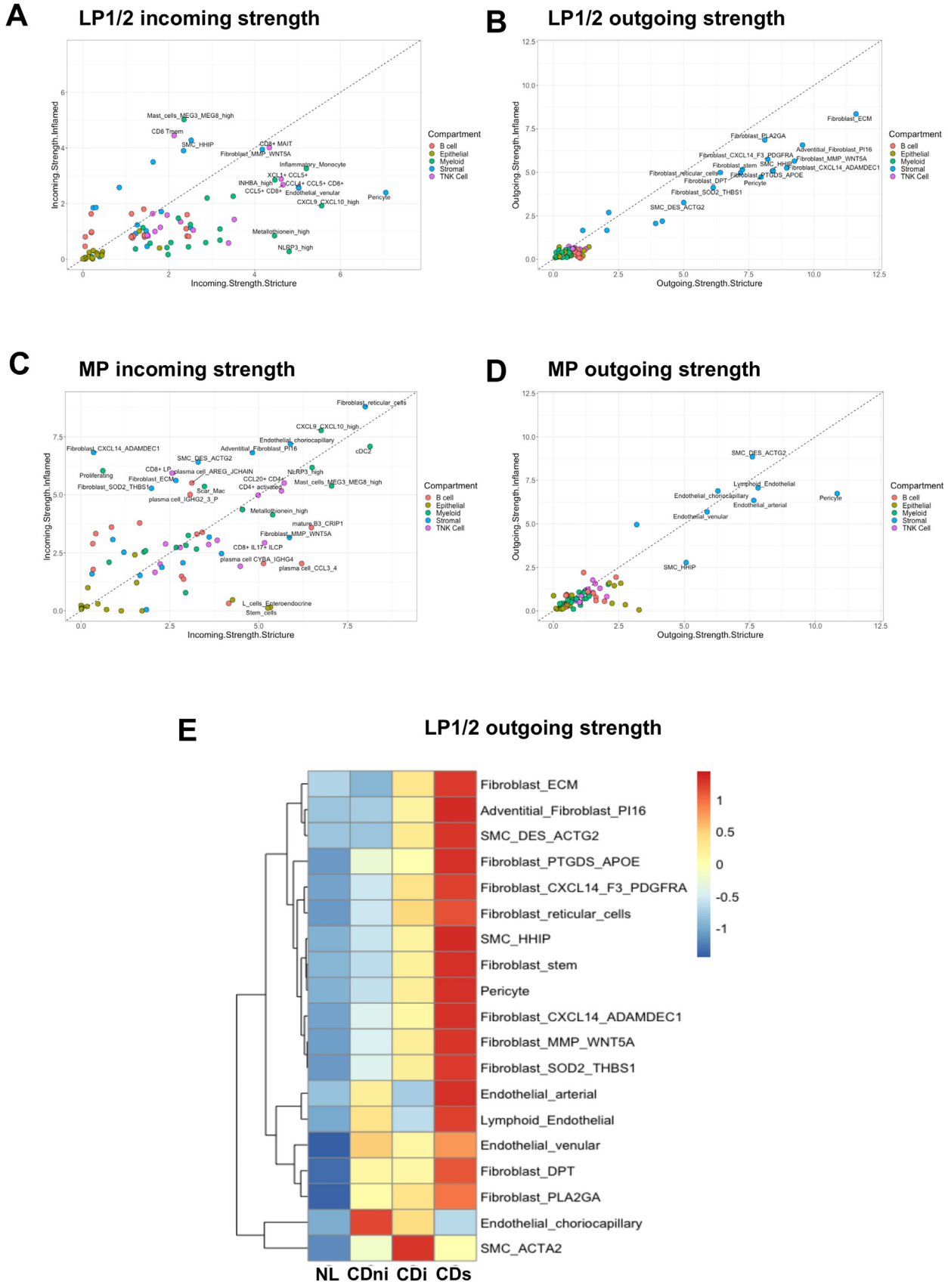

Figure 3. Cell-cell interaction analysis of the full scRNAseq atlas by tissue segment and layer. (*A* and *B*) Scatterplot of the incoming (*A*) and outgoing (*B*) interaction strength for CDs vs CDi sections in the LP1/2 layers calculated using cellChat.[14] Each dot represents a cell type (*C* and *D*). Scatterplot of the incoming (*C*) and outgoing (*D*) interaction strength for CDs vs CDi sections in the MP layers calculated using cellChat. Each dot represents a cell type. (*E*) Heatmap of outgoing signal strength of the stromal compartment by cell type and segment, scaled by cell type. *Red* indicates high- and *blue* indicates low-signal strength.

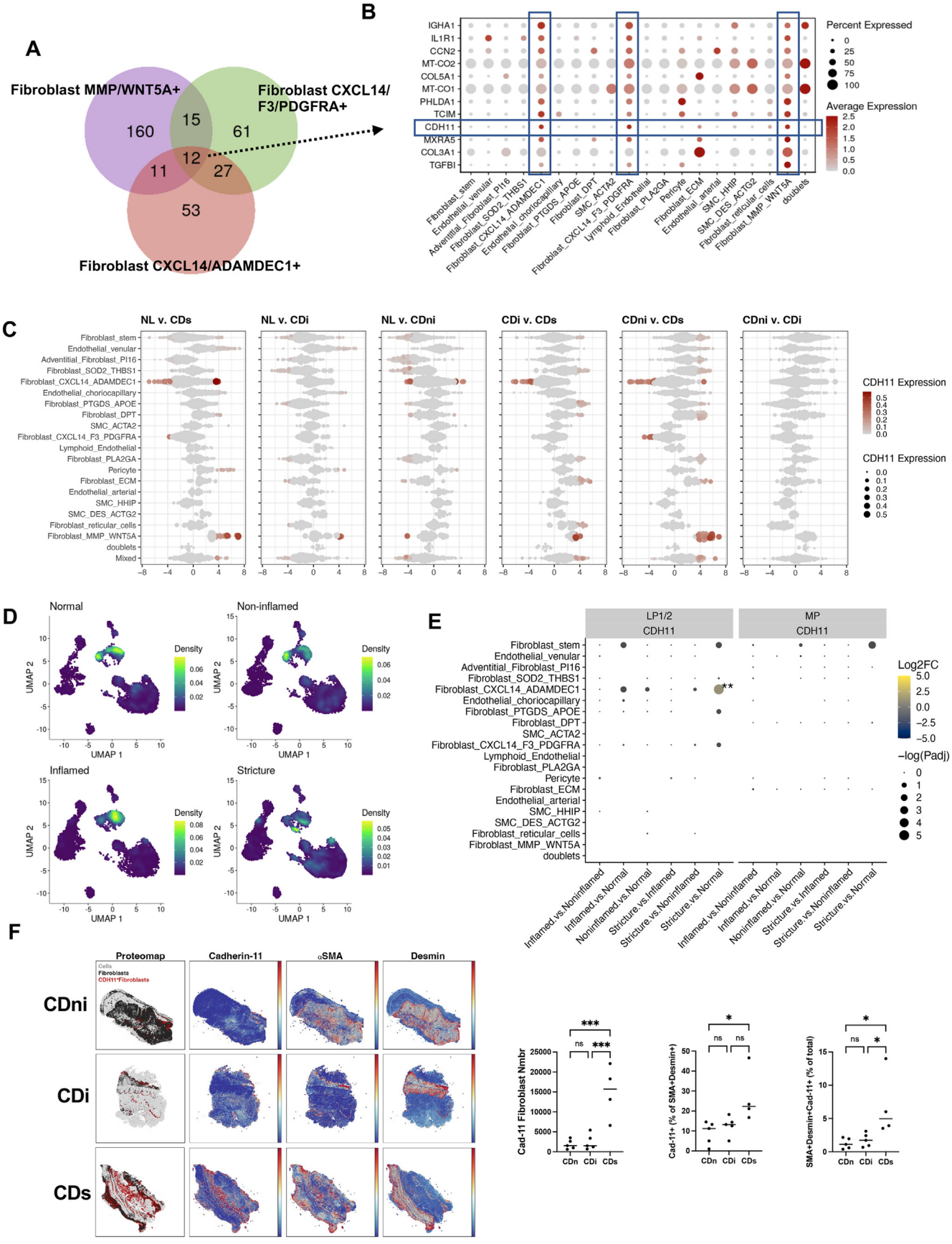
A
Fibroblast MMP/WNT5A+
Fibroblast CXCL14/ F3/PDGFRA+
Fibroblast CXCL14/ADAMDEC1+
160
15
61
12
11
27
53
B
IGHA1
IL1R1
CCN2
MT-CO2
COL5A1
MT-CO1
PHLDA1
TCIM
CDH11
MXRA5
COL3A1
TGFBI
Fibroblast_stem
Endothelial_venular
Adventitial_Fibroblast_PI16
Fibroblast_SOD2_THBS1
Fibroblast_CXCL14_ADAMDEC1
Endothelial_choriocapillary
Fibroblast_PTGDS_APOE
Fibroblast_DPT
SMC_ACTA2
Fibroblast_CXCL14_F3_PDGFRA
Lymphoid_Endothelial
Fibroblast_PLA2GA
Pericyte
Fibroblast_ECM
Endothelial_arterial
SMC_HHIP
SMC_DES_ACTG2
Fibroblast_reticular_cells
Fibroblast_MMP_WNT5A
doublets
Percent Expressed
0
25
50
75
100
Average Expression
2.5
2.0
1.5
1.0
0.5
0.0
C
NL v. CDs
NL v. CDi
NL v. CDni
CDi v. CDs
CDni v. CDs
CDni v. CDi
Mixed
CDH11 Expression
D
Normal
Non-inflamed
Inflamed
Stricture
UMAP 1
UMAP 2
Density
E
LP1/2
CDH11
MP
CDH11
Log2FC
5.0
2.5
0.0
−2.5
−5.0
−log(Padj)
Inflamed.vs.Noninflamed
Inflamed.vs.Normal
Noninflamed.vs.Normal
Stricture.vs.Inflamed
Stricture.vs.Noninflamed
Stricture.vs.Normal
F
Proteomap
Cadherin-11
αSMA
Desmin
Cells
Fibroblasts
CDH11+Fibroblasts
CDni
CDi
CDs
Cad-11 Fibroblast Nmbr
Cad-11+ (% of SMA+Desmin+)
SMA+Desmin+Cad-11+ (% of total)
CDn
CDi
CDs
ns
***
*

CDH11 Emerges as a Dominant Cell Surface Molecule in CD Strictures

Our cell-cell interaction analysis revealed a dominant role for fibroblasts as pathobiologically relevant "signal senders" as well as "receivers." We hence queried molecules that may mediate fibroblast-fibroblast interactions by focusing on 3 populations that were over-represented in the isolated LP1/2 compared with MP layers and either increased in CDs segments (MMP/WNT5A+) or showed major transcriptional changes in CDs (CXCL14/PDGFRA+ and CXCL14+/ADAMDEC1+). When interrogating overlapping gene signatures of these populations, we detected 12 shared markers (Figure 4*A* and *B*), of which only *CDH11* is expressed on the cell surface and in addition is highly selective to fibroblasts (Supplementary Figure 4*C*). When analyzing *CDH11* expression across stromal cell types, LP1/2 layer neighborhoods that had a high *CDH11* expression also had an increased abundance or differentially expressed genes in CDs, making this a marker for stromal cells enriched in CDs (Figure 4*C*). A shift in the density of *CDH11* expression is noted in parallel to disease progression from NL, through CDni and CDi, to CDs (Figure 4*D*). Of relevance, CDH11+ stromal cells are not only increased in abundance in CDs, but *CDH11* is increased in CXCL14/ADAMDEC1+ fibroblasts on a per cell basis (Figure 4*E*). Automated cyclic immunofluorescence analysis on FFPE intestinal tissue sections confirmed robust up-regulation of CDH11 in the mucosa/submucosa in CDs with minor expression in the MP. CDH11 was coexpressed with α-SMA and desmin (DES) and the frequency of CDH11/α-SMA/DES+ cells compared with total cells or within the α-SMA/DES+ fraction increased in CDs (Figure 4*F*).

CDH11 is Up-Regulated in IBD Tissues

Underscoring the pathophysiological relevance of CDH11 in CDs, we found up-regulation of its gene and protein expression in full-thickness ileal CDs, ileal CD nonstricturing (CDns), and colonic UC compared with the NL colon tissues (Figure 5*A* and *B*), with the most pronounced increase (up to 35-fold) found in CDs. As mentioned in Supplementary Methods, for the validation experiments we grouped CDi and CDni together, termed CDns. This was done because the CDni portions of the resection are very small in size and not amendable to cell isolation in sufficient numbers for the experiments. To be consistent across the validation experiments we used the grouping of CDns and CDs across all experiments beginning with Figure 5. UC samples were included in the target validation program to serve as an intestinal inflammatory control. Dual-immunolabeling with markers of mesenchymal, endothelial, and epithelial cells and leukocytes colocalized CDH11 with α-SMA and vimentin in the mucosa and submucosa, and enrichment in a subfraction of DES-positive cells (Figure 5*C*, Supplementary Figure 6) compatible with high CDH11 expression by myofibroblasts. Expression of CDH11 was low in the muscularis propria and did not change based on the disease phenotype (data not shown). Minimal to no colocalization of CDH11 was found with CD45, CD68, E-cadherin, and CD31 (Supplementary Figure 6), indicating that immune cells, including tissue resident macrophages, are minimal contributors to CDH11 expression in the inflamed gut.

A prespecified NanoString panel comprising 13 genes associated with fibrotic diseases in an independent cohort of FFPE full-thickness intestinal tissues revealed overlap between NL (colon), UC (colon), and CDns (ileum) in a principal component analysis and heatmap. Some genes expressed in CDs (ileum) were separated from the other groups, compatible with up-regulation of *CDH11* (Figure 5*D* and *E*). Considering all groups combined *CDH11* was positively correlated with COL1A1, COL1A2, COL3A1, CTGF, SPP1, TIMP1, and SERPINE. The same was true for the CD samples combined except for CTGF. When assessing UC, CDns, and CDs separately, *CHD11* correlated with COL1A1, COL1A2, and COL3A1 in all of them. Interestingly, *CHD11* only correlated with MMP2 in the NL tissues (Figure 5*F*).

IBD Myofibroblasts Express Increased Levels of CDH11

Investigation of various human intestinal cells revealed that CDH11 was expressed by HIMF and human intestinal muscle cells, but not epithelial cells, lamina propria mononuclear cells, or human intestinal microvascular endothelial cells (Figure 5*G*). Analysis of a publicly available scRNAseq dataset[7] from UC mucosal biopsies confirmed that CDH11 mean and percent expression clusters in the stromal compartment, with the strongest signal in inflammatory fibroblasts. The epithelial and immune cell compartments did not express CDH11 (Supplementary Figure 6*H*). CDH11 expression was higher in CD HIMF compared with NL (Figure 5*H*).

Modulation of CDH11 Activity Affects Myofibroblast ECM Production

We next investigated the effect of CDH11 loss-of-function in HIMF with blocking antibody H1M1[15] or

Figure 4. *CDH11* is a potential regulator of intestinal fibrosis. (*A*) Venn diagram showing overlap of significant markers for CXCL14/ADAMDEC1+, CXCL14/F3/PDGFRA+, and MMP/WNT5A+ fibroblasts. (*B*) Dot plot of 12 overlapping markers from *A*. (*C*) Differential abundance beeswarm plots from miloR analysis of LP1/2 layers in stromal compartment with neighborhoods colored by *CDH11* expression. Only significantly differentially abundant neighborhoods show *CDH11* expression. (*D*) UMAP plots of *CDH11* expression density in stromal compartment split by segment (NL, CDni, CDi, and CDs). (*E*) Dot plot demonstrating *CDH11* pseudobulk differential expression by cell type. Significance is shown by size and denoted by **(adjusted *P* value <.01). Only contrasts with a significant adjusted *P* value (<.05) show log fold-change color. (*F*) Cyclic immunofluorescence of intestinal FFPE section using vimentin, α-SMA, and DES antibodies (Supplementary Table 4). Automated quantification is indicated. Data are presented as mean ± standard deviation. *$P < .05$; **$P < .001$.

silencing RNA (siRNA) knockdown (KD). We developed a novel medium throughput ECM deposition assay where the deposited (v soluble or gene expression) ECM is automatically measured (see the Methods section). Treatment with H1M1 reduced deposition of fibronectin (FN) and ColI/III in a dose-dependent manner in NL (colon), UC

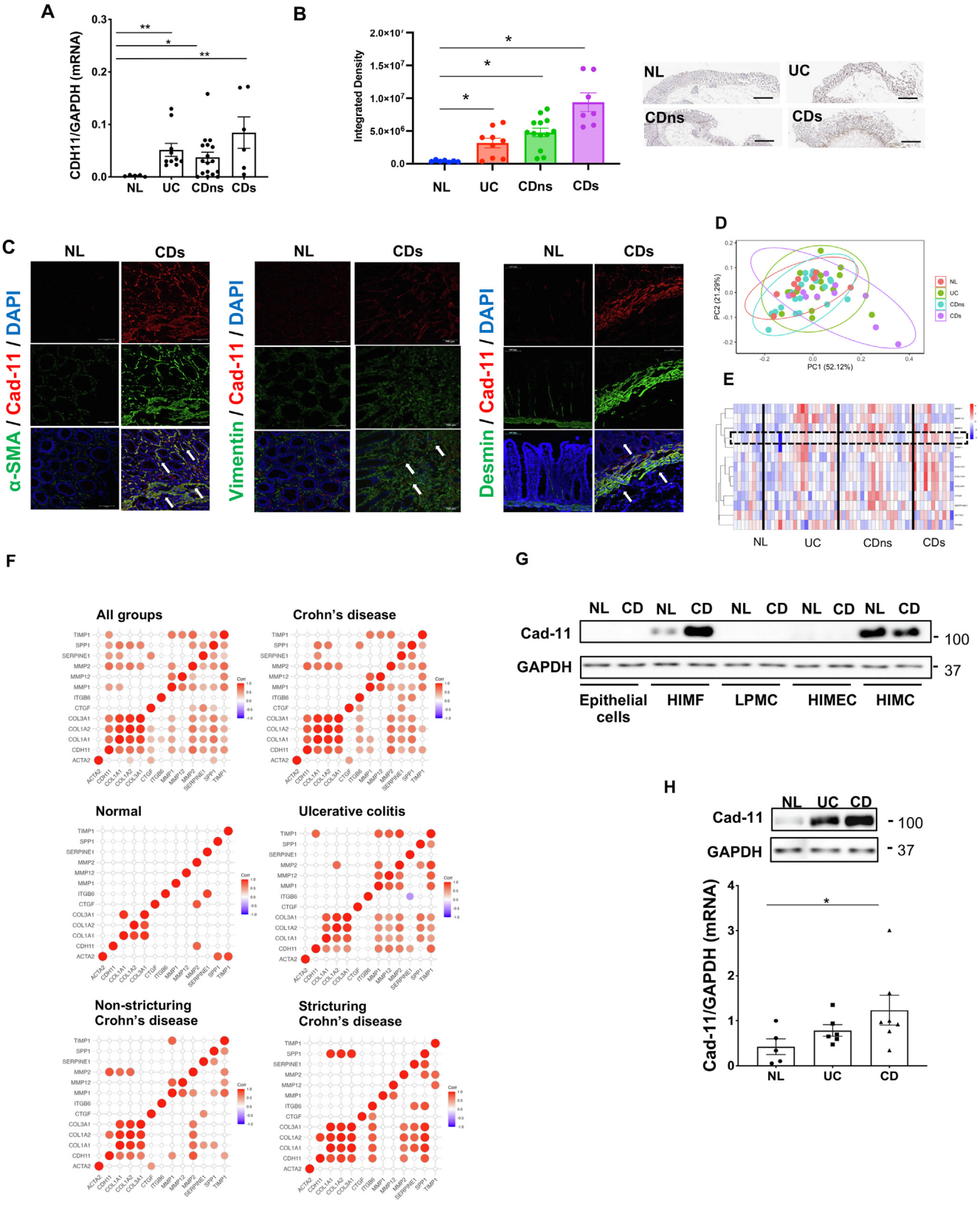

(colon), CDns (ileum), and CDs (ileum) HIMF (Figure 6*A* and *B*). CDH11 KD markedly down-regulated its expression and decreased cellular level of FN (Figure 6*C*). In contrast, CDH11 gain-of-function by extracellular recombinant human CDH11 domain-Fc chimera ("CDH11 activator")[16] resulted in a dose-dependent increase of FN and ColI/III deposition by NL, UC, CDns, and CDs HIMF (Figure 6*A* and *B*), an effect comparable with TGF-β1, the strongest profibrotic activator of HIMF (Figure 6*B*). CDH11 activator only affected HIMF function when it was plate-bound but not in soluble form (data not shown). Given the analysis of scRNAseq suggesting a dominant signal sender role of CDs fibroblasts, we analyzed the HIMF secretome with and without CDH11 activation (Figure 6*D* and *E*, Supplementary Figure 7, Supplementary Table 7). Also, 332 proteins were significantly different on CDH11 activation, with 179 up-regulated and 153 down-regulated. CDH11 activation up-regulated secretion of multiple core matrisome proteins suggesting a broad profibrotic effect. Pathway enrichment analysis indicated the up-regulation of multiple proteins and signaling pathways related to inflammation, suggesting a proinflammatory effect of CDH11 (Figure 6*E*). The detailed analysis of the secretome is found in Supplementary Figure 7 and Supplementary Table 7.

Global Gene Expression Mediated by CDH11

Next-generation RNA sequencing (RNAseq) in NL HIMF with and without gene KD of *CDH11* resulted in differential expression of 475 genes (260 down-regulated, 215 up-regulated; Figure 6*F* and *G*). The top up-regulated and down-regulated genes, correlation analysis, and gene enrichment analysis with *CDH11* confirm correlation of *CDH11* with ECM deposition, remodeling, and cell proliferation (Supplementary Figure 8*A*–*C*, Supplementary Tables 8 and 9). *CDH11* correlated with a majority (116/161) of known matrisome genes, including FN1, COL1A1, COL3A1, COL6A1, and others. The top 30 genes with the strongest correlation with *CDH11* can be found in Supplementary Figure 8*D* and the correlation between *CDH11* and collagens and fibronectin in Supplementary Figure 8*E*. *CDH11* KD up-regulated expression of multiple proinflammatory genes (IL1A, IL1B, CCL20, and IL33), but at the same time down-regulated expression of other proinflammatory genes (CXCL12, CXCL14, or CCL8). Among modulation of multiple pathways, *CDH11* KD revealed a robust down-regulation of sphingosine and FAK signaling (Figure 6*H*, Supplementary Tables 8–10). As a result of this data and to validate scRNAseq as a tool for therapeutic target discovery, we chose to interrogate our stromal populations of interest to CDs (both CXCL14+ and the WNT5A+ fibroblasts) in our scRNAseq dataset. Corroborating the next-generation sequencing (NGS) results, sphingosine metabolism was strongly linked with *CDH11* expression in these populations (Figure 6*I*). Modulation of sphingosine and FAK signaling pathways by inhibition of AKT, mTOR, Pi3K, and FAK with selective small molecules led to amelioration of CDH11-induced ECM deposition, functionally confirming the relevance of these pathways to CDH11 profibrotic function (Figure 6*J*). Importantly, the observed effects were not due to increased cell death because at the end of the experiments cell viability was 100% (Supplementary Figure 9*A*).

Functional Ablation of CDH11 Improves Experimental Intestinal Fibrosis

We last investigated the therapeutic potential of CDH11 inhibition in vivo by using a total knockout of CDH11 (Cdh11-KO) in the DSS-induced fibrosis model of colitis.[15] The clinical score was reduced in Cdh11-KO throughout the course of DSS administration (Figure 7*A*). Cdh11-KO showed no difference in inflammation compared with WT mice (Figure 7*B*), but reduced picrosirius red, ColI, FN staining (Figure 7*C*), and reduced thickening of the muscularis mucosa, submucosa, and muscularis propria (Figure 7*D*). Cdh11-KO mice displayed a reduction in gene expression of *IL6* and tumor necrosis factor (TNF) compared with WT mice (Figure 7*E*).

We then examined the effect of CDH11 blocking antibody H1M1 in DSS fibrosis. H1M1 pharmacokinetics (PK) study established the dose of 0.5 mg/mouse every other day as optimal (Supplementary Figure 9), reaching a minimum plasma H1M1 level of >200 μg/mL to achieve optimal efficacy.[17] On preventive administration of H1M1, the clinical score was reduced during DSS administration and post-DSS recovery (Figure 7*F*). H1M1 did not reduce severity of

Figure 5. CDH11 expression is up-regulated in the intestine of patients with IBD. (*A*) Expression of *CDH11* messenger RNA in fresh full-thickness sections. *CDH11* level was normalized by GAPDH messenger RNA expression (n = 43). (*B*) Immunohistochemistry of full-thickness intestinal resection tissues immunolabelled with CDH11 and quantified by integrated density values (IDV). (Representative images shown here, *scale bars:* 800 μm.) (*C*) Full-thickness sections of patients with NL and patients with CDs were dual-immunolabeled for CDH11 (*red*) and either α-SMA, vimentin, or desmin (*green*). Representative confocal images with the full panel being available in Supplementary Figure 6. *Arrows* point to colocalization of CDH11 with myofibroblast markers. Representative for n = 4 per group. (*D* and *E*) Principal components analysis and heatmap analysis of ECM-related gene expression in FFPE tissue using a prespecified NanoString nCounter panel and normalized to housekeeping genes. Ellipses indicate 95% confidence intervals. Separation of the gene panel was noted in CDs compared with the other groups (n = 59). (*F*) Correlograms showing statistically significant correlations for relative abundance of ECM-related gene expression in FFPE tissue using a prespecified NanoString nCounter panel (Spearman correlation, $P \leq .05$). *Red dots* indicate positive correlation. (*G*) Expression of CDH11 was examined using immunoblotting analysis in the following primary human intestinal cell types: intestinal epithelial cells; HIMF; lamina propria mononuclear cells (LPMC); human intestinal microvascular endothelial cells (HIMEC); and human intestinal muscle cells (HIMC). (*H*) Expression of CDH11 protein in HIMF isolated from patients with CD, patients with UC, and non-IBD controls was compared using immunoblotting analysis and densitometric quantification, Data are presented as mean ± standard deviation (n = 17). Data are presented as mean ± standard deviation (n = 8–12). *$P < .05$.** $P < .01$.

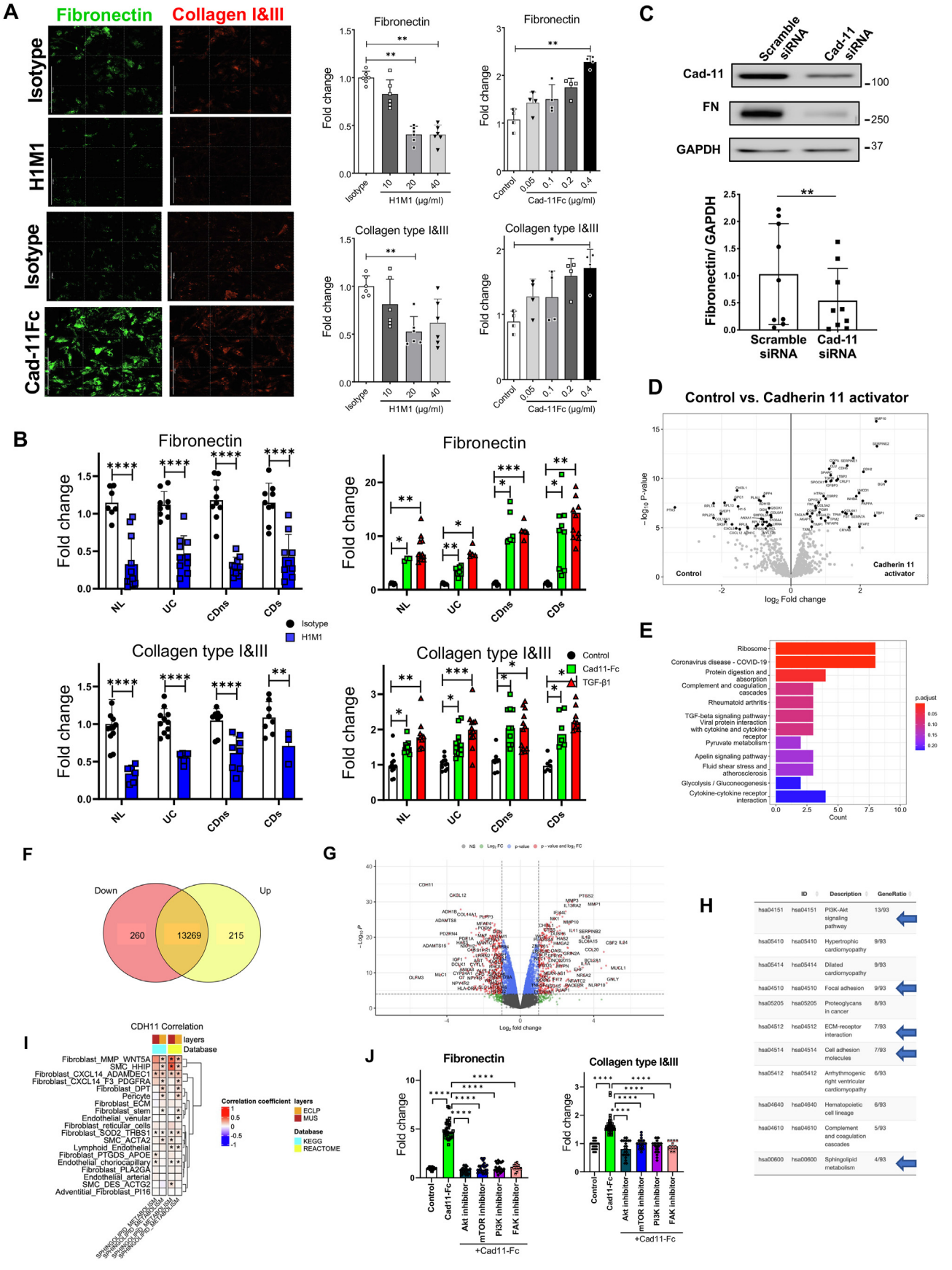
A
Fibronectin
Collagen I&III
Isotype
H1M1
Isotype
Cad-11Fc
Fibronectin
Fold change
H1M1 (μg/ml)
Cad-11Fc (μg/ml)
Collagen type I&III
B
NL
UC
CDns
CDs
Isotype
H1M1
Control
Cad11-Fc
TGF-β1
C
Scramble siRNA
Cad-11 siRNA
Cad-11
FN
GAPDH
-100
-250
-37
Fibronectin/ GAPDH
D
Control vs. Cadherin 11 activator
Control
Cadherin 11 activator
log2 Fold change
E
Ribosome
Coronavirus disease - COVID-19
Protein digestion and absorption
Complement and coagulation cascades
Rheumatoid arthritis
TGF-beta signaling pathway
Viral protein interaction with cytokine and cytokine receptor
Pyruvate metabolism
Apelin signaling pathway
Fluid shear stress and atherosclerosis
Glycolysis / Gluconeogenesis
Cytokine-cytokine receptor interaction
p.adjust
Count
F
Down
Up
260
13269
215
G
Log2 fold change
H
ID
Description
GeneRatio
hsa04151 PI3K-Akt signaling pathway 13/93
hsa05410 Hypertrophic cardiomyopathy 9/93
hsa05414 Dilated cardiomyopathy 9/93
hsa04510 Focal adhesion 9/93
hsa05205 Proteoglycans in cancer 8/93
hsa04512 ECM-receptor interaction 7/93
hsa04514 Cell adhesion molecules 7/93
hsa05412 Arrhythmogenic right ventricular cardiomyopathy 6/93
hsa04640 Hematopoietic cell lineage 6/93
hsa04610 Complement and coagulation cascades 5/93
hsa00600 Sphingolipid metabolism 4/93
I
CDH11 Correlation
layers
Database
Correlation coefficient
ECLP
MUS
KEGG
REACTOME
J
Fibronectin
Collagen type I&III
Control
Cad11-Fc
Akt inhibitor
mTOR inhibitor
PI3K inhibitor
FAK inhibitor
+Cad11-Fc

inflammation[18] (Figure 7*G*), but reduced development of fibrosis as measured using picrosirius red, FN1, and ColI staining (Figure 7*H*) and reduced muscularis propria thickening (Figure 7*I*). H1M1 also reduced gene expression of *TNF* and showed a trend for reduced *IL6* expression (Figure 7*J*).

Discussion

Organ fibrosis is a universal response to multiple pathologic conditions of inflammatory, neoplastic, or degenerative nature.[5] Depending on its extent and location, fibrosis has serious consequences that become the primary cause of symptoms and disease evolution as well as choice of therapeutic intervention. This is well exemplified by the management of fibrosis-induced stricture formation in CD, which is still very challenging due to a limited understanding of the underlying cellular and molecular mechanisms.[2] To overcome this limitation, we analyzed the transcriptome of 409,001 intestinal cells from 20 patients and generated the first full-thickness CDs scRNAseq atlas. Our dataset provides novel information on the epithelial, immune, and stromal compartments and enables the characterization of cell type–specific differences along tissue segments and layers. These data point to *CDH11* as a key driver of stricturing CD and a putative therapeutic target.

Our results contribute several new key findings for CDs. First, the major differences between noninflamed, inflamed, and strictured bowel segments at the cell type and transcriptional level are found in the LP1/2 fraction, reflecting the isolated mucosa and submucosa. Far fewer alterations were detected in the MP of CDs despite its marked thickening and contribution to obstructive symptoms.[2] This may be explained by post-transcriptional regulation of human intestinal muscle cells proliferation and activation or by the use of tissue samples in a late process of stricture formation. Various stromal cell types were exclusive to the LP1/2 or MP fractions, which highlights the unique features of each tissue layer.

Second, we identified fibroblasts as major signal-sending hubs in CDs. This is highly relevant, as to date it was unclear which mechanisms drive the progression from pure inflammation to fibrostenosis and whether progression is driven by inflammation-dependent or -independent processes.[2] Being major signal senders, this puts fibroblasts in the center of strategies to block transition of inflammation to fibrosis or to directly prevent or eliminate fibrosis.

Third, our work identified in CDs an abundance of MMP/WNT5A+ fibroblasts, a cell type expressed exclusively in the LP1/2 but not the MP fractions. This fibroblast type matches a cell known as inflammatory fibroblast (IL13RA2/IL11+)[7] from the mucosa of patients with UC resistant to anti-TNF treatment. One could speculate that the presence of MMP/WNT5A+ and the reported association with anti-TNF resistance is mediated by the presence of fibrosis. We also found a CXCL14+ fibroblast population coexpressing either PDGFRA or ADAMDEC1 displaying the most pronounced transcriptional changes in CDs, and hence of functional relevance. CXCL14+ fibroblasts have been associated with increased ECM production[19] and CXCL14 itself has profibrotic properties.[20] ADAMDEC1 is critical in the fibroblastic response to tissue remodeling and healing during colitis[21] and PDGFRA+ fibroblasts display a proliferative phenotype and are a major source of collagen.[22,23]

Based on the prominent role of fibroblasts in CDs signaling, the differences largely restricted to the LP1/2 fraction, the over-representation of distinct fibroblast types, and the strong contribution to transcriptional changes in CDs, we sought a unifying molecule and identified CDH11 as the only cell surface receptor shared by the CXCL14+ and MMP/WNT5A+ fibroblasts. Although also expressed in macrophages, CDH11 is primarily responsible for mediating homophilic stromal cell-cell interactions,[24–27] is up-regulated in fibrotic disorders of the lung,[24] liver,[25] skin,[26] and intestine,[27] and its inhibition attenuates fibrosis in multiple animal models.[25] This raises the prospect of using CDH11 blockade to prevent or treat CD-associated intestinal fibrosis.

In support of this, we confirmed in CDs a marked up-regulation of CDH11 messenger RNA and protein expression,[27] and correlation of CDH11 gene expression with

Figure 6. CDH11 regulates the fibrogenic phenotype of HIMFs. CDH11 was either inhibited in HIMF isolated from subjects using CDH11 blocking antibody (H1M1) or specific silencing RNA (siRNA) to CDH11 or activated by CDH11 activator (Cad11-Fc). (*A*) HIMF from NL intestinal tissue were exposed to different doses of H1M1 or Cad11-Fc and ECM deposition (FN and ColI/III) was assayed using the ECM deposition assay (n = 6 per group). Representative immunofluorescence images are shown. *Scale bar*: 1000 μm. (*B*) HIMF from the patient groups NL, UC, CDns, and CDs were exposed to H1M1 (20 μg/mL) or Cad11-Fc (0.4 μg/mL), respectively, and assayed using the ECM deposition assay. TGF-β1 (1 ng/mL) was used as a positive control (n = 12). (*C*) KD of CDH11 was performed in HIMF and CDH11 and FN expression was determined using immunoblotting and densitometric quantification (n = 18) (for primer details, please see Supplementary Table 5). (*D*) Annotated volcano plot of secreted proteins with up-regulated (*right*) and down-regulated (*left*) proteins with and without CDH11 activation in HIMF NL (n = 9 for each group). (*E*) Protein enrichment analysis of the HIMF NL secretome in response to CDH11 activation. (*F*) Significantly up-regulated (*yellow*) and down-regulated (*red*) genes on *CDH11* siRNA KD in HIMF NL (n = 4 each for the scrambled control and KD groups). (*G*) Annotated volcano plot with up-regulated (*right*, *red*) and down-regulated (*left*, *red*) genes on *CDH11* KD. (*H*) Kyoto Encyclopedia of Genes and Genomes (KEGG) pathway enrichment analysis on *CDH11* KD. (*I*) Heatmap of the correlation of CDH11 normalized expression with sphingosine signaling. Ucell scores derived from KEGG and Reactome databases in mesenchymal cell types in our scRNAseq dataset. Significant *P* values (unadjusted) are denoted with a *. (*J*) HIMF NL were exposed to hIgG1 (control) or Cad11-Fc (0.4 μg/mL) with or without compound inhibitors (GSK690693 [Akt inhibitor, 5 μmol/L]; mTOR Inhibitor XI [mTOR Inhibitor, 0.25 μmol/L]; LY-294,002 hydrochloride [Pi3K inhibitor, 30 μmol/L]; Y15, 1,2,4,5-benzenetetramine tetrahydrochloride [FAK inhibitor, 5 μmol/L]) and assayed using the ECM deposition assay (n = 18). Data are presented as mean ± standard deviation. *$P < .05$; **$P < .01$; ***$P < .001$; ****$P < .0001$.

hallmark profibrotic genes. CDH11 was predominantly expressed in fibroblasts in bowel tissue, isolated primary intestinal cells, and in scRNAseq. CDH11+ cells were more frequent in CDs and on a per cell basis CDH11 was up-regulated in MMP/WNT5A+ inflammatory fibroblasts. By using a novel ECM deposition assay we also showed that

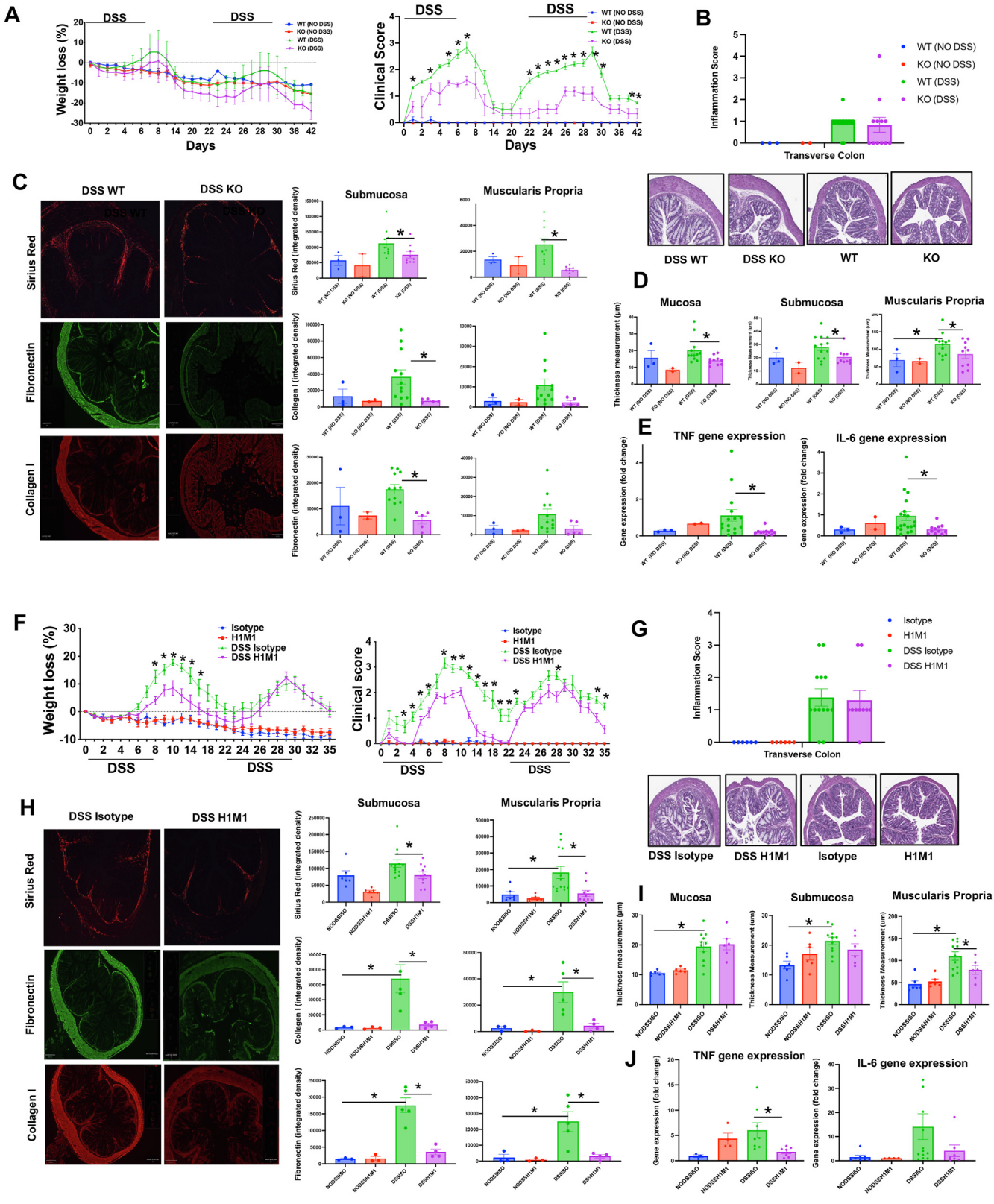

CDH11 has strong profibrotic properties in vitro comparable in magnitude with those of TGF-b1. Measuring actual ECM deposition instead of gene expression is important because it most closely reflects the in vivo situation. Using proteomics and next-generation sequencing, we uncovered a broad profibrotic effect of CDH11 in vitro and the potential mechanism of sphingosine and FAK signaling, a finding that was confirmed in our scRNAseq dataset and functionally validated using small molecule inhibitors in HIMF.

Importantly, a pharmacologic (antibody-mediated) or genetic inhibition of CDH11 decreased intestinal fibrosis in vivo without any adverse effects after prolonged administration. This is consistent with previously published data in 2,4,6-trinitrobenzene sulfonic acid (TNBS) colitis in CDH11-KO mice[27] and, in addition to providing a different fibrosis model, adds the successful administration of a blocking antibody. In our experimental fibrosis model, however, we were only able to appreciate an anti-inflammatory property on the intestinal gene expression level for *TNF* and *IL6*, but not on histopathologic inflammation scoring. This may indicate that the antifibrotic effects outweigh any anti-inflammatory effects in vivo.

Our study has several limitations. Although the CD tissues were rigorously phenotyped and we were able to procure 3 distinct segments per patient (CDni, CDi, CDs), we were not successful in procuring NL ileal control tissues. Hence, our NL controls were derived from the colon. This, however, had no bearing on the overall results of this investigation. The cell types that were over-represented in CDs or transcriptionally active in CDs were found irrespective of using colon NL or ileal CDni as controls. We, however, cannot exclude that the described differences between NL and CDni were due to the origin of the tissue in the intestine (colon vs small bowel). In the in vitro validation experiments we used HIMF derived from the colon of UC and NL subjects as controls. UC HIMF were deliberately chosen as inflammatory controls to the CD ileal fibroblasts. Strikingly, no functional difference in response to CDH11 modulation was noted between the different groups. Of note and consistent with the notion that UC is a progressive disease,[2] CDH11 was up-regulated in UC and its gene expression correlated with profibrotic gene expression. The DSS experimental fibrosis model exhibits fibrosis in the colon and not the small bowel. How well the ECM expression in this model reflects ileal CD-like fibrosis is not known, which, on the one hand, can be considered a limitation of its use. On the other hand, together with the CDH11 expression and functional validation data, it underscores CDH11 as a molecule with potential therapeutic utility in CD- and UC-associated fibrosis.

Given the large amount of data we focused our initial efforts on a systematic analysis strategy that revealed CDH11 as a potential target. This does not exclude discovery or validation of any other additional targets and, in fact, our intent with this work is to make this data available to the research community for this purpose. For example, one interesting finding is the strong incoming signal strength of conventional dendritic cells (cDC2) in the MP of CDs segments, which already led to inception of an exploratory experimental program evaluating their interactions.

In conclusion, by developing a detailed single-cell atlas of noninflamed, inflamed, and strictured autologous CD tissue segments, characterizing the strong profibrotic activity of specific mesenchymal cell subsets in the mucosa and submucosa, and identifying CDH11 as a widely expressed cell surface molecule essential for ECM production, we uncovered novel cellular and molecular mechanisms involved in CDs and CDH11 as a potential therapeutic target.

Supplementary Material

Note: To access the supplementary material accompanying this article, visit the online version of *Gastroenterology* at www.gastrojournal.org, and at http://doi.org/10.1053/j.gastro.2023.07.014.

References

1. Ng SC, Shi HY, Hamidi N, et al. Worldwide incidence and prevalence of inflammatory bowel disease in the 21st century: a systematic review of population-based studies. Lancet 2017;390:2769–2778.
2. Rieder F, Fiocchi C, Rogler G. Mechanisms, management, and treatment of fibrosis in patients with inflammatory bowel diseases. Gastroenterology 2017;152:340–350.e6.

Figure 7. Blockade or genetic ablation of CDH11 attenuates chronic DSS-induced colitis in mice. Cdh11 null (KO) mice and WT littermates were subjected to 2 cycles of DSS administration (2%) followed by post-DSS recovery. (*A*) The severity of DSS-induced colitis was evaluated by measuring the body weight loss and calculating the clinical score (n = 12 per group). Colonic sections were fixed and stained with H&E for histologic examination. (*B*) The inflammation score was determined using H&E sections by an IBD pathologist in a blinded fashion. (*C*) The severity of fibrosis was evaluated through Sirius red staining, Col1, or FN immunolabeling and quantified using integrated density measurements for the submucosa and the muscularis propria separately. (*D*) Thickness of the intestinal layers was measured for mucosa, submucosa, and muscularis propria. (*E*) Gene expression of TNF and IL6 in intestinal tissues. WT mice were subjected to 2 cycles of DSS administration (2%) followed by post-DSS recovery. Cdh11 blocking antibody H1M1 or isotype antibody were given daily starting on day 1 of the experiment. (*F*) Severity of DSS-induced colitis was evaluated by measuring the body weight loss and calculating the clinical score (n = 10 per group). (*G*) Inflammation score was determined using H&E sections by an IBD pathologist in a blinded fashion. (*H*) Severity of fibrosis was evaluated through picrosirius red staining, Col1, or FN immunolabeling and quantified using integrated density measurements for the submucosa and the muscularis propria separately. (*I*) Thickness of the intestinal layers was measured for mucosa, submucosa, and muscularis propria. (*J*) Gene expression of TNF and IL6 in intestinal tissues. Data are presented as mean ± standard error of mean. *$P < .05$.

3. Peyrin-Biroulet L, Oussalah A, Williet N, et al. Impact of azathioprine and tumour necrosis factor antagonists on the need for surgery in newly diagnosed Crohn's disease. Gut 2011;60:930–936.
4. **Kugathasan S**, **Denson LA**, **Walters TD**, et al. Prediction of complicated disease course for children newly diagnosed with Crohn's disease: a multicentre inception cohort study. Lancet 2017;389:1710–1718.
5. **Henderson NC**, **Rieder F**, **Wynn TA**. Fibrosis: from mechanisms to medicines. Nature 2020;587:555–566.
6. Powell DW, Pinchuk IV, Saada JI, et al. Mesenchymal cells of the intestinal lamina propria. Annu Rev Physiol 2011;73:213–237.
7. Smillie CS, Biton M, Ordovas-Montanes J, et al. Intra- and inter-cellular rewiring of the human colon during ulcerative colitis. Cell 2019;178:714–730.e22.
8. **Kinchen J**, **Chen HH**, **Parikh K**, et al. Structural remodeling of the human colonic mesenchyme in inflammatory bowel disease. Cell 2018;175:372–386.e17.
9. Kong L, Pokatayev V, Lefkovith A, et al. The landscape of immune dysregulation in Crohn's disease revealed through single-cell transcriptomic profiling in the ileum and colon. Immunity 2023;56:444–458.
10. Daperno M, D'Haens G, Van Assche G, et al. Development and validation of a new, simplified endoscopic activity score for Crohn's disease: the SES-CD. Gastrointest Endosc 2004;60:505–512.
11. Geboes K, Riddell R, Ost A, et al. A reproducible grading scale for histological assessment of inflammation in ulcerative colitis. Gut 2000;47:404–409.
12. Chiorean MV, Sandrasegaran K, Saxena R, et al. Correlation of CT enteroclysis with surgical pathology in Crohn's disease. Am J Gastroenterol 2007;102:2541–2550.
13. Bon H, Hales P, Lumb S, et al. Spontaneous extracellular matrix accumulation in a human in vitro model of renal fibrosis is mediated by alphaV integrins. Nephron 2019;142:328–350.
14. Jin S, Guerrero-Juarez CF, Zhang L, et al. Inference and analysis of cell-cell communication using CellChat. Nat Commun 2021;12:1088.
15. McArthur JG. Humanized antibodies targeting the EC1 domain of Cadherin-11 and related compositions and methods. US Patent US8940300B2. USA: Adheron Therapeutics Inc, 2011. Available at: https://patents.google.com/patent/US8940300B2/en.
16. Pittet P, Lee K, Kulik AJ, et al. Fibrogenic fibroblasts increase intercellular adhesion strength by reinforcing individual OB-cadherin bonds. J Cell Sci 2008;121:877–886.
17. Schroer AK, Bersi MR, Clark CR, et al. Cadherin-11 blockade reduces inflammation-driven fibrotic remodeling and improves outcomes after myocardial infarction. JCI Insight 2019;4:e131545.
18. Xuan L, Ren L, Han F, et al. Cytomegalovirus infection exacerbates experimental colitis by promoting IL-23 production. Inflammation 2020;43:326–335.
19. van Kuijk K, McCracken IR, Tillie R, et al. Human and murine fibroblast single cell transcriptomics reveals fibroblast clusters are differentially affected by ageing, and serum cholesterol. Cardiovasc Res 2023;119:1509–1523.
20. Li L, Li Q, Wei L, et al. Chemokine (C-X-C motif) ligand 14 contributes to lipopolysaccharide-induced fibrogenesis in mouse L929 fibroblasts via modulating PPM1A. J Cell Biochem 2019;120:13372–13381.
21. **Jasso GJ**, **Jaiswal A**, Varma M, et al. Colon stroma mediates an inflammation-driven fibroblastic response controlling matrix remodeling and healing. PLoS Biol 2022;20:e3001532.
22. Yao L, Rathnakar BH, Kwon HR, et al. Temporal control of PDGFRalpha regulates the fibroblast-to-myofibroblast transition in wound healing. Cell Rep 2022;40:111192.
23. Raslan AA, Pham TX, Lee J, et al. Single cell transcriptomics of fibrotic lungs unveils aging-associated alterations in endothelial and epithelial cell regeneration. bioRxiv 2023. Preprint. https://doi.org/10.1101/2023.01.17.523179.
24. Black M, Milewski D, Le T, et al. FOXF1 inhibits pulmonary fibrosis by preventing CDH2-CDH11 cadherin switch in myofibroblasts. Cell Rep 2018;23:442–458.
25. Pedroza M, To S, Smith J, et al. Cadherin-11 contributes to liver fibrosis induced by carbon tetrachloride. PLoS One 2019;14:e0218971.
26. Pedroza M, Welschhans RL, Agarwal SK. Targeting of cadherin-11 decreases skin fibrosis in the tight skin-1 mouse model. PLoS One 2017;12:e0187109.
27. Franze E, Monteleone I, Laudisi F, et al. Cadherin-11 is a regulator of intestinal fibrosis. J Crohns Colitis 2020;14:406–417.

Author names in bold designate shared co-first authorship.

Received April 3, 2023. Accepted July 3, 2023.

Correspondence
Address correspondence to: Florian Rieder, MD, Department of Gastroenterology, Hepatology & Nutrition, Digestive Diseases and Surgery Institute, 9500 Euclid Avenue, Cleveland, Ohio, 44195. e-mail: riederf@ccf.org.

Acknowledgments
The authors thank Dr Judith Drazba, Dr John Peterson, Andrelie Branicky, Apryl Helmick, and Bridget Besse from the LRI Microscopy and Image Core of the Cleveland Clinic for help in confocal microscopy and image analysis. The authors thank Dr Belinda Willard and Dr Isaac Ampong from the Metabolomic and Proteomics Core of the Cleveland Clinic for support of the proteomics analysis. The authors appreciate the support of the Genomics Core of the University of Chicago for next-generation sequencing. The authors thank Pfizer Inflammation and Immunology Research Units' Fibrosis Discovery Group and Systems Immunology group for helpful comments and support, as well as Pfizer's cellular and optical microscopy technology center for their imaging support. The authors acknowledge the support of the Departments of Colorectal Surgery and Pathology of the Cleveland Clinic. The authors thank the contribution of the Cleveland Clinic Center for Global Translational IBD. The authors also deeply appreciate the contribution of patients who donated the tissues.

Pranab K. Mukherjee, Quang Tam Nguyen, Jiannan Li, Shuai Zhao, and Stephen M. Christensen contributed equally to this work.

CRediT Authorship Contributions
Pranab Kumar Mukherjee, PhD (Conceptualization: Equal; Data curation: Lead; Formal analysis: Equal; Investigation: Equal; Methodology: Equal; Project administration: Equal; Supervision: Equal; Visualization: Lead; Writing – original draft: Equal; Writing – review & editing: Equal).

Quang Tam Nguyen, PhD (Data curation: Equal; Formal analysis: Equal; Writing – review & editing: Supporting).

Jiannan Li, MD (Conceptualization: Equal; Data curation: Equal; Formal analysis: Equal; Funding acquisition: Equal; Writing – review & editing: Supporting).

Shuai Zhao, MS (Data curation: Equal; Writing – review & editing: Equal).

Stephen M. Christensen, PhD (Data curation: Equal; Formal analysis: Equal; Writing – original draft: Equal; Writing – review & editing: Equal).

Gail A. West, BS (Conceptualization: Supporting; Data curation: Supporting; Writing – review & editing: Supporting).
Jyotsna Chandra, PhD (Data curation: Equal; Writing – review & editing: Supporting).
Ilyssa O. Gordon, MD (Data curation: Equal; Writing – review & editing: Equal).
Sinan Lin, MD (Data curation: Supporting; Writing – review & editing: Equal).
Jie Wang, PhD (Data curation: Supporting; Writing – review & editing: Supporting).
Ren Mao, MD (Data curation: Supporting; Writing – review & editing: Supporting).
Douglas Czarnecki, HSD (Data curation: Supporting; Writing – review & editing: Supporting).
Carla Rayan, MD (Data curation: Supporting; Writing – review & editing: Supporting; Regulatory: Supporting).
Idan Goren, MD (Data curation: Supporting; Formal analysis: Supporting; Methodology: Supporting; Writing – review & editing: Supporting).
Suhanti Banerjee, MS (Data curation: Supporting; Formal analysis: Supporting; Methodology: Supporting; Writing – review & editing: Supporting).
Prerna Kotak, BS (Data curation: Supporting; Writing – review & editing: Supporting).
Thomas Plesec, MD (Data curation: Supporting; Writing – review & editing: Supporting).
Samir Lal, PhD (Data curation: Equal; Formal analysis: Equal; Writing – review & editing: Equal).
Thomas Fabre, PhD (Data curation: Equal; Writing – review & editing: Supporting).
Shoh Asano, PhD (Data curation: Supporting; Formal analysis: Supporting; Writing – review & editing: Supporting).
Kathryn Bound, BS (Data curation: Supporting; Writing – review & editing: Supporting).
Kevin Hart, PhD (Data curation: Supporting; Writing – review & editing: Supporting).
Chanyoung Park, BS (Data curation: Supporting; Formal analysis: Supporting; Writing – review & editing: Supporting).
Robert Martinez, PhD (Data curation: Supporting; Writing – review & editing: Supporting; Oversight: Supporting).
Ken Dower, PhD (Data curation: Supporting; Writing – review & editing: Supporting).
Thomas A. Wynn, PhD (Oversight/Advisory: Supporting).
Shaomin Hu, MD (Data curation: Supporting; Writing – review & editing: Supporting).
Nayden Naydenov, PhD (Data curation: Supporting; Writing – review & editing: Supporting).
Martin Decaris, PhD (Data curation: Supporting; Writing – review & editing: Supporting).
Scott Turner, PhD (Writing – review & editing: Supporting; Oversight/Advisory: Supporting).
Stefan D. Holubar, MD (Data curation: Supporting; Writing – review & editing: Supporting).
Scott R. Steele, MD (Data curation: Equal; Writing – review & editing: Supporting).
Claudio Fiocchi, MD (Funding acquisition: Equal; Writing – review & editing: Equal).
Andrei I. Ivanov, PhD (Writing – review & editing: Supporting).

Conflicts of interest

These authors disclose the following: I.O.G. received funding from UCB, Celgene, Gossamer, and Pliant. S.D.H. was a consultant to Shionogi and Takeda. S.M.C., S.L., T.F., S.A., K.B., K.H., R.M., K.D., T.W., and K.M.K. are employees of Pfizer, Inc and may hold stock equity. C.P. was a visiting graduate scholar at Pfizer, Inc. P.K., M.D., and S.T. are employees of Pliant Inc. C.F. received speaker fees from UCB, Genentech, Sandoz, and Janssen and he is a consultant for Athos Therapeutics, Inc. F.R. was a consultant to AbbVie, Adnovate, Agomab, Allergan, Arena, Astra-Zeneca, Boehringer-Ingelheim, Celgene/BMS, CDISC, Celsius, Cowen, Ferring, Galapagos, Galmed, Genentech, Gilead, Gossamer, Granite, Guidepoint, Helmsley, Horizon Therapeutics, Image Analysis Limited, Index Pharma, Landos, Jannsen, Koutif, Mestag, Metacrine, Mopac, Morphic, Organovo, Origo, Pfizer, Pliant, Prometheus Biosciences, Receptos, RedX, Roche, Samsung, Sanofi, Surmodics, Surrozen, Takeda, Techlab, Teva, Theravance, Thetis, UCB, Ysios, and 89Bio. The remaining authors disclose no conflicts.

Funding

This work was supported by the Helmsley Charitable Trust through the Stenosis Therapy and Anti-Fibrotic Research (STAR) Consortium (to F.R.), the Crohn's and Colitis Foundation Fellowship Award (No. 648334 to J.L.), and Pliant and Pfizer Inc through sponsored research agreements. No sponsor had any involvement in study design, collection or interpretation of data. Pfizer Inc supported bioinformatic analysis in collaboration with the Cleveland Clinic.

Data Availability

The transcriptomic datasets will be shared on request at time of publication. Please contact the corresponding author for any inquiries. The Cleveland Clinic agrees to use the National Institutes of Health's Federal Demonstration Partnership (FDP) Data Transfer and Use Agreement (DTUA) template to share the data, which can be found at https://thefdp.org/default/committees/research-compliance/data-stewardship/. For any other inquiries please contact the corresponding author.